Sensors and Materials, Vol. 38, No. 1 (2026) 227–241
MYU Tokyo

S & M 4296

Method of Analyzing the Optimal Composite Vegetation Index Based on Multisensor Information and Multivegetation Index Combinations

YongSuk Kim,[1] Do-Young Jung,[2*] and LongYi Zhang[1]

[1]Department of Landscape Architecture, Dong-A University, Busan 49315, Republic of Korea
[2]Department of Highway and Transportation Research,
303-504, 28, Nuwon-ro, Nowon-gu, Seoul 01600, Republic of Korea

(Received August 25, 2025; accepted November 13, 2025)

Keywords: multisensor information, composite vegetation index, drone, *NDVI*, *RENDVI*, *NDWI*, *PRI*

In this study, we investigated the variation in vegetation index in Hwado, South Korea, from 2022 to 2025. The analysis utilized time-series data collected from multiple sensors mounted on drones. The primary vegetation indices used for the analysis included the normalized difference vegetation index (*NDVI*) (*V*1), red-edge *NDVI* (*RENDVI*) (*V*2), normalized difference water index (*NDWI*) (*V*3), and photochemical reflectance index (*PRI*) (*V*4). These indices were specifically applied to assess vegetation health across various periods (A, B, C, and D). Notably, the indices *V*1 and *V*2 during Period A demonstrated a higher vitality than the other periods and indices. To overcome the limitations of single vegetation indices, we analyzed 44 unique combinations of multiple vegetation indices, together referred to as the composite vegetation index (*CVI*). In this study, we aimed to evaluate and assess areas of healthy vegetation both quantitatively and qualitatively. The results showed that combinations (1), (7), and (11) during Period A had the highest vegetation vitality, with more than 80% of the area covered by healthy vegetation. During all periods, combinations (1) and (7), each consisting of *V*1 and *V*2, consistently demonstrated a high percentage of healthy area. As a result, Combination (7) in Period A was identified as the optimal composite vegetation index (Optimal *CVI*) in this study. The proposed *CVI* accurately measures vegetation vitality by effectively reflecting the specific characteristics of the study area and integrating multisensor information. It can be utilized for health analysis in various types of forest.

1. Introduction

Recently, the societal awareness of climate change and environmental issues has increased, and consequently, the importance of precisely monitoring changes in the health and distribution of vegetation has attracted increasing attention.[1,2] In particular, vegetation information is the basis for critical decision-making in various fields, including agriculture, forestry, and

*Corresponding author: e-mail: jdy@kict.re.kr
https://doi.org/10.18494/SAM5887

ISSN 0914-4935
https://myukk.org/

environmental management.[3] Traditional ground-based surveys face physical and economic limitations in covering large areas or capturing time-series changes.[4,5] Consequently, the use of remote sensing technologies for efficient and wide-range monitoring has gradually increased.

Among remote sensing technologies, unmanned aerial vehicles (UAVs) have become increasingly important in precision agriculture and forest monitoring owing to their ability to acquire high-resolution images at low altitudes.[6] UAV-based remote sensing is actively used to detect and manage forest diseases[7] such as pine wilt disease (PWD).[8–11] It can overcome the limitations of traditional methods and enable the rapid assessment of the health of large forests.

For vegetation monitoring, vegetation indices are key tools; they are quantitative indicators of the vitality, density, and health of vegetation based on combinations of reflectance in specific wavelength bands. The normalized difference vegetation index (*NDVI*), a typical vegetation index, has been widely used to indicate vegetation density and health. However, it has the limitation of saturating in high-density vegetation areas.[12] To overcome this limitation, various vegetation indices have been developed, including red-edge *NDVI* (*RENDVI*), normalized difference water index (*NDWI*), and photochemical reflectance index (*PRI*). On the basis of these indices, studies have been conducted to capture multifaceted information, such as chlorophyll content, water stress, and photosynthetic efficiency.[13–15]

However, single vegetation indices are limited by their inability to completely reflect the complex physiological and structural characteristics of vegetation. In the early stages of PWD infection, subtle and complex symptoms appear, including changes in chlorophyll content, water stress, and reduced photosynthetic efficiency.[16] These changes are difficult to effectively detect with a single index. An approach utilizing multisensor information (e.g., various spectral bands such as rgb, nir, and red-edge) and combining and analyzing multiple vegetation indices is required to more accurately assess these complex vegetation conditions.[17] This approach can reflect the physical and physiological characteristics of vegetation through various spectral information; thus, it can compensate for the limitations of conventional single indices and provide a more comprehensive understanding of vegetation health.

In this context, in this study, we used multisensor information to present a new composite vegetation index (*CVI*) that can effectively detect areas with high vegetation vitality and compensate for the limitations of conventional vegetation indices (*NDVI*, *RENDVI*, *NDWI*, and *PRI*). We aimed to propose a more accurate and efficient method for monitoring changes in vegetation health and distribution. This will ultimately contribute to providing basic data for the early diagnosis of forest diseases and sustainable forest management.

2. Data, Materials, and Methods

2.1 Study area and data

The study area was an inhabited island called Hwado in Geoje (city), Gyeongsangnam-do (province), South Korea. The area is dominated by simple pine forests, primarily *Pinus thunbergii*, covering more than 80% of the total area, which makes it favorable for multispectral image-based vegetation index analysis. The area has been reported to have dead trees owing to

PWD for several years, and owing to the island's remote location, access for personnel and equipment is limited. In recent years, methods to control PWD have relied on aerial surveillance-based forecasting and drone-based remote sensing rather than on the mechanical control of the disease. These environmental characteristics make Hwado suitable for UAV-based multispectral image analysis and vegetation index applications, which aligns with the objectives of this study. Thus, we selected it as our experimental site (Fig. 1). Table 1 presents the circumstances under which images and data were acquired at four time points from 2022 to 2025. These time points are categorized as Periods A, B, C, and D. The main reason for selecting these time periods is that South Korea has a temporal characteristic of high vegetation vitality (health) from April to October.

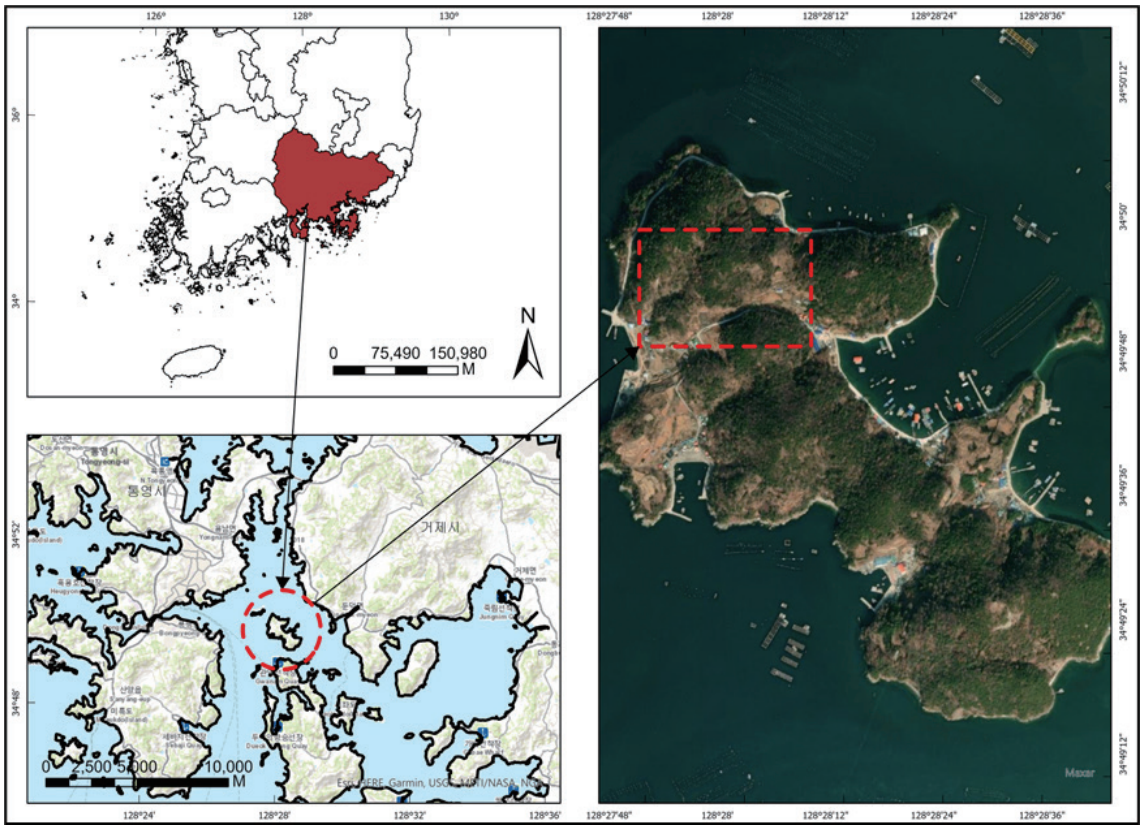

Fig. 1. (Color online) Study area.

Table 1
Drone information.

UAV	Period classification	Shooting date	Sensor	Band	Sentera 6×	Mavic 3M
DJI Matrice 300 RTK	A	Aug. 11, 2022	Sentera 6× Multispectral Sensor	Blue	475 ± 15 nm	
	B	Oct. 14, 2022		Green	550 ± 10 nm	560 ± 16 nm
				Red	670 ± 15 nm	650 ± 16 nm
	C	Mar. 16, 2023		Red-Edge	715 ± 5 nm	730 ± 16 nm
				NIR	840 ± 10 nm	860 ± 26 nm
Mavic 3M	D	May 2, 2025	Mavic 3M	RGB	IR cut at 650 nm	20 MP RGB

In this study, we used a DJI Matrice 300 RTK drone, Sentera 6× Multispectral Sensor (Sentera 6× sensor), and Mavic 3M to obtain data. The image-capturing conditions were set at 150 m above ground level and a longitudinal overlap (70%), and the sensor information was acquired at a certain altitude by applying the digital surface model (DSM) information. Table 1 presents the sensor equipment and information for each spectral band.

2.2 Research flow diagram

Drone multisensor images were used to derive the optimal *CVI* on the basis of various combinations of vegetation indices. Figure 2 shows the research flow diagram. The vegetation indices *NDVI*, *RENDVI*, *NDWI*, and *PRI* were analyzed, and changes in these indices were quantitatively examined by geographic information system (GIS)-based spatial analysis. The final *CVI* was determined on the basis of the 44 distributions of vegetation vitality analyzed using combinations of multiple vegetation indices.

2.3 Vegetation indices and vegetation index combination network

The experimental area is a coniferous forest with a high density of *Pinus thunbergii*. This island area has a high concentration of dead trees owing to PWD. Owing to its simple vegetation and minimal external disturbances, the area is very suitable for evaluating the accuracy of vegetation index-based disease detection. Moreover, seasonal vegetation responses appear clearly in Hwado owing to the maritime climate, and the decline in photosynthetic activity caused by disease outbreaks in image (sensor) information can be clearly detected. In particular, this area is classified as a vulnerable area for disease control owing to limited access; thus, remote early surveillance and forecasting based on drone images and vegetation indices are necessary. In this study, we selected four basic vegetation indices suitable for the experimental area for analyses.

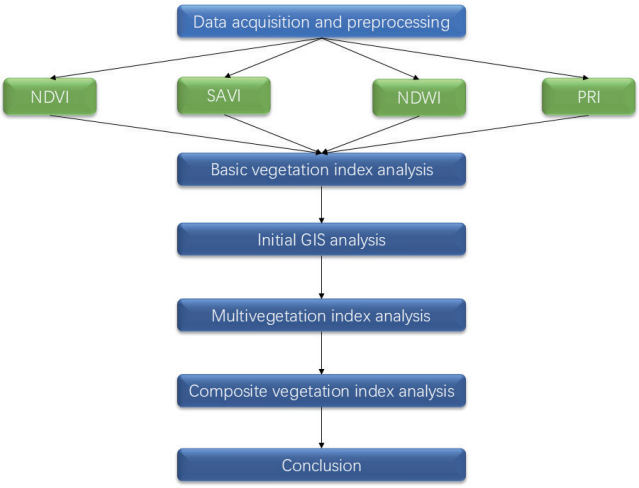

Fig. 2. (Color online) Research flow diagram.

NDVI is one of the most widely used vegetation indices to indicate the photosynthetic activities of plants. Healthy plants show low reflectance in the red wavelength band of visible light owing to high chlorophyll absorption and reflectance in the NIR wavelength band owing to internal scattering caused by their chlorophyll structure.

$$NDVI = \frac{NIR - RED}{NIR + RED} \tag{1}$$

RENDVI is a vegetation index that uses the red-edge wavelength band. This part is characterized by a sharp increase in reflectance from the visible red wavelength band (approximately 680 nm) to the NIR wavelength band (approximately 750 nm). This domain is characterized by a highly sensitive response to changes in the chlorophyll content and nitrogen status of plants. *RENDVI* was developed to compensate for the limitation of *NDVI* of saturating in dense vegetation. It is particularly sensitive to changes in chlorophyll content, making it useful for detecting plant stress or early-stage disease.

$$RENDVI = \frac{NIR - Red\ Edge}{NIR + Red\ Edge} \tag{2}$$

NDWI, proposed by Gao,[18] utilizes the NIR (approximately 800–900 nm) and shortwave infrared (SWIR; approximately 1550–1750 nm) bands to directly measure the water content of plant leaves. As the NIR band shows a high reflectance owing to the cellular structure of vegetation, the combination of these two bands shows a highly sensitive response to leaf water content, making it effective for assessing water stress. The Sentera 6× sensor can acquire data for blue, green, red, red-edge, and NIR bands but does not include SWIR bands. Accordingly, we used the NIR and green bands (approximately 550 nm) to analyze *NDWI* in this study.

$$NDWI = \frac{Green - NIR}{Green + NIR} \tag{3}$$

PRI was proposed by Gamon *et al*.;[19] it uses changes in reflectance in a very narrow wavelength band between 531 and 570 nm to primarily estimate a plant's photosynthetic radiation use efficiency (RUE) in real time. Changes in reflectance in this wavelength band are caused by the activity of the xanthophyll cycle of carotenoid pigments. It is closely related to the phenomenon of non-photochemical quenching, wherein plants dissipate excess light energy.[19] Considering the characteristics of very narrow bandwidths, which are required to calculate *PRI*, such as 531 or 570 nm, we set *PRI* using Eq. (4) for the Sentera 6× sensor.

$$PRI = \frac{Green - RED}{Green + RED} \tag{4}$$

The four vegetation indices used in this study were selected as each one represents the different physiological and structural characteristics of vegetation, enabling a comprehensive

analysis of vegetation condition.[20] By using these four indices together, a variety of information, such as vegetation cover, pigment content, water content status, and photosynthetic efficiency, can be extracted through complex analysis.

We followed a four-step spatial analysis procedure using ArcGIS Pro to quantitatively calculate the total area and area by category on the basis of the results of the analysis of vegetation index. First, we used the Raster Calculator to categorize the continuous vegetation index raster into four bins based on predefined thresholds, and we converted them to raster integer values to ensure that categorical (gridcode) attributes can be assigned. Second, we used the "Raster to Polygon" tool to convert the pixel-based raster data into polygonal data in a vector form (polygonal shape), thereby transforming data with a spatial unit that enables area calculation. Third, the area field for each polygon object was created and automatically calculated using the "Calculate Geometry" tool with the generated polygon data. Finally, we used the "Summary Statistics" function to aggregate the area totals by category (gridcode) to quantitatively calculate the area distribution of each vegetation index bin relative to the total area.

As shown in Fig. 3, vegetation indices (Group 1) are categorized as follows: $V1 = NDVI$, $V2 = RENDVI$, $V3 = NDWI$, and $V4 = PRI$. For the categories (Groups 2 and 3) based on the combination of vegetation indices, we showed each combination as (1), (2), (3), ..., (11). We produced 11 combination equations: (1) = $V1 + V2$, (2) = $V1 + V3$, (3) = $V1 + V4$, ..., (10) = $V2 + V3 + V4$, and (11) = $V1 + V2 + V3 + V4$.

3. Results

3.1 Analysis of basic vegetation indices

The images used for the analysis of basic vegetation indices were preprocessed using Pix4D Mapper. We applied the four vegetation indices ($V1$, $V2$, $V3$, and $V4$) to the periods of image

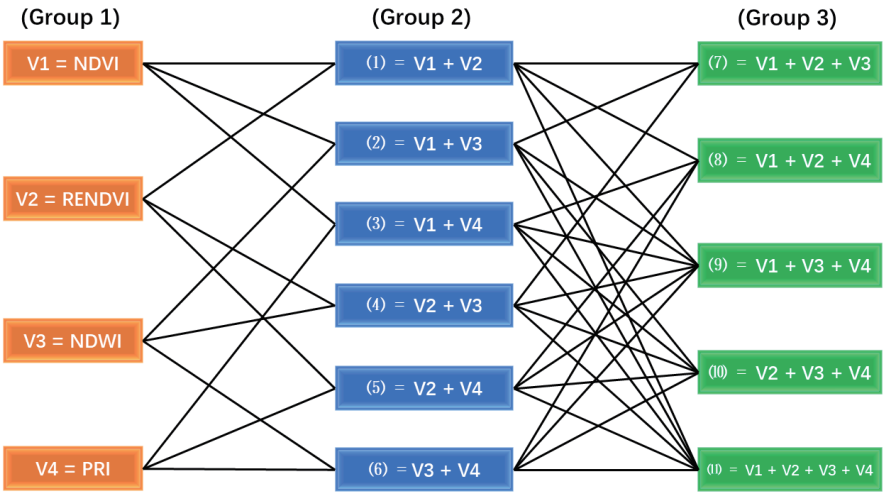

Fig. 3. (Color online) Combination network of vegetation indices.

acquisition (A, B, C, and D, respectively) and presented 16 index distributions, as shown in Fig. 4. Considering the presence of a certain amount of noise in the experimental area, we excluded noise less than 0.5% of total area as it had no significant effect on analysis. In Table 2, we presented the vegetation indices according to each combination equation using a legend for five vegetation levels [vegetation levels: green (L5), blue-green (L4), yellow (L3), orange (L2), and red (L1)]. The areas corresponding to green and blue-green (L5 and L4), which represent healthy vegetation, were calculated and summed to assess the vegetation vitality of the corresponding combination.

Table 2 shows the vegetation index area by period, and Fig. 4 shows four of the 16 basic vegetation indices. Vegetation indices closer to 1 (green) indicate higher vitality, whereas those closer to −1 (red) indicate lower vitality. *NDVI* shows that the overall healthy vegetation area (L4 + L5) was approximately 92234 m^2 in Period A, indicating very high vitality. *RENDVI* revealed that the blue-green areas (L4) were approximately 45060 m^2 (28%) during Period C, indicating low vitality, and approximately 69363 m^2 (43%) in Period D, indicating high vitality. *NDWI* showed that the L1 areas were the largest in Periods A (66744 m^2) and B (66273 m^2), suggesting that desiccation (lack of moisture) was a factor in the decline in vitality. *PRI* reflects the photosynthesis of plants[21] and is characterized by high values in summer and low values in fall and winter. Notably, *PRI* increased during Period A.

Figure 5 shows a heatmap of the area distribution of vegetation index by classifying periods (A, B, C, and D) and vegetation levels (L1–L5). Healthy vegetation is higher in Periods A (*V*1,

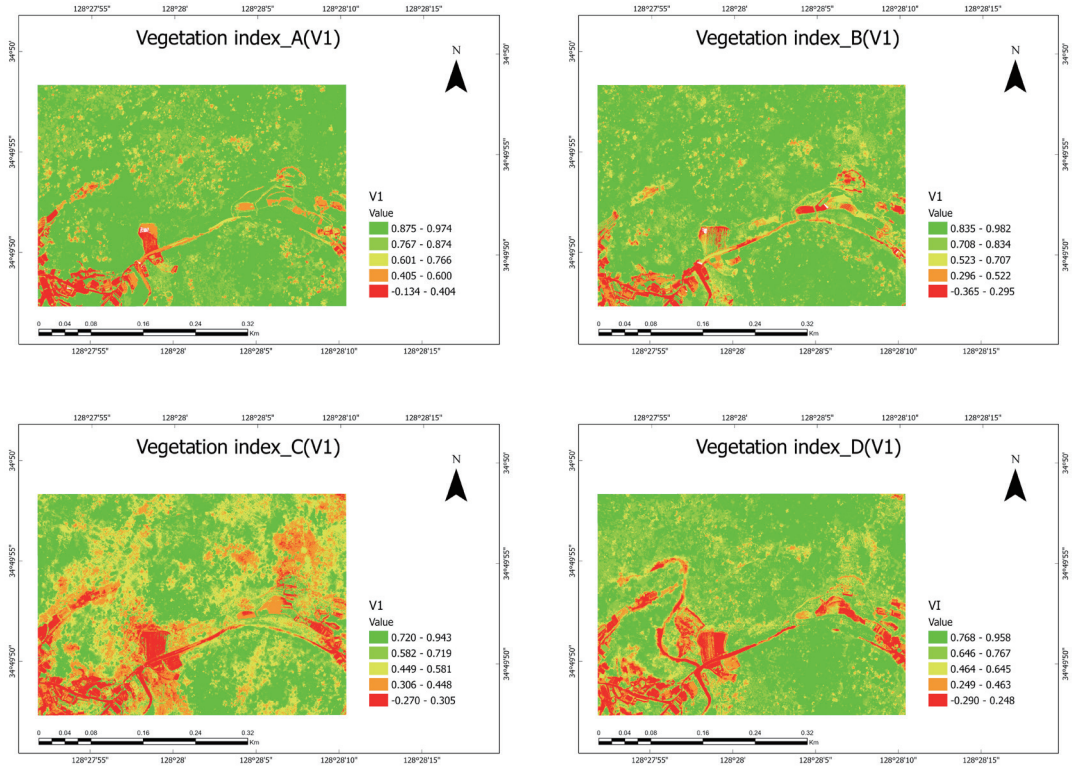

Fig. 4. (Color online) Basic vegetation index by period.

Table 2
(Color online) Basic vegetation index analysis. (unit: m^2)

Period	Vegetation index				
	Vegetation level	*V*1	*V*2	*V*3	*V*4
A	Green (L5)	92234	45241	3282	41023
	Blue-green (L4)	42405	61305	7601	61324
	Yellow (L3)	1119	35083	14600	31869
	Orange (L2)	8280	9382	67853	16018
	Red (L1)	5835	9094	66744	9717
B	L5	84300	42100	3634	3634
	L4	46585	65836	8200	8199
	L3	15824	32467	19900	19900
	L2	7580	12742	62071	62074
	L1	5673	6943	66273	66284
C	L5	40076	33035	4210	12993
	L4	37717	45060	13945	25044
	L3	42362	48467	33296	33881
	L2	26799	23778	56270	50922
	L1	13132	9750	52337	37216
D	L5	64685	21926	4989	42697
	L4	53268	69363	12806	45057
	L3	19484	53888	20739	38001
	L2	1096	14911	66299	23941
	L1	11685	4	55260	10397

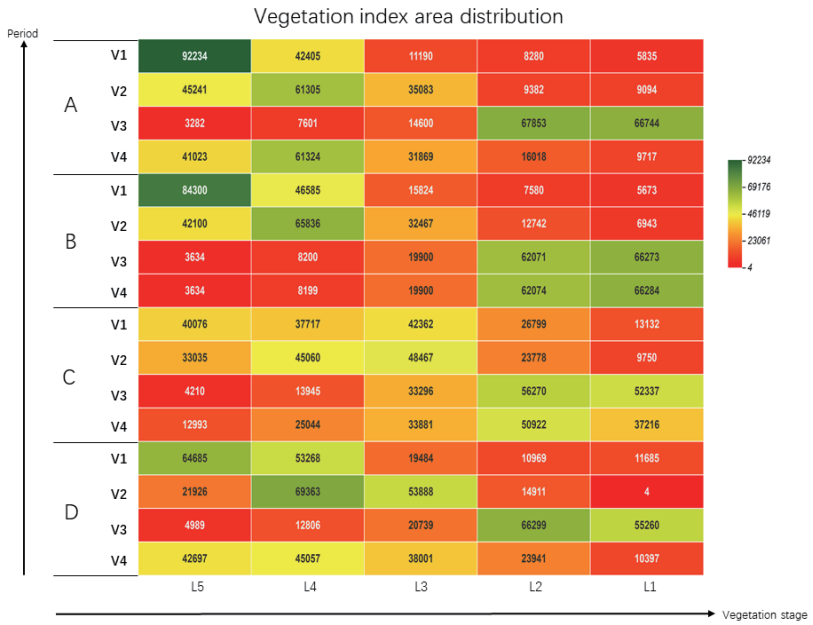

Fig. 5. (Color online) Basic vegetation indices (Group 1).

*V*2, and *V*4), B (*V*1 and *V*2), and D (*V*1). Conversely, in Period C, *V*3 and *V*4 show low vitality overall. This may be ascribed to seasonal factors. Nonetheless, this also suggests that the water content of plants, as indicated by *NDWI*, and the growth rate of vegetation affected by photosynthetic efficiency, as indicated by *PRI*, are low.

3.2 Analysis of multivegetation index combinations

In the analysis of the multivegetation index combinations, the total number of combinations based on Groups 2 and 3 is 44, as shown in Fig. 3. We conducted qualitative and quantitative analyses for each combination. In Fig. 6, we showed the vegetation distribution for only six out of the 44 combinations of multiple vegetation indices owing to the limited space in this study. Table 3 presents the results of the area of the combined vegetation indices by period, and we analyzed the correlation of the combination equations for healthy vegetation (L4 and L5).

The analysis of vegetation area showed that combinations (1), (7), and (11), which contained *V*1 for Period A, were found to have a healthy vegetation area (L4 + L5) of 80% or more. Period

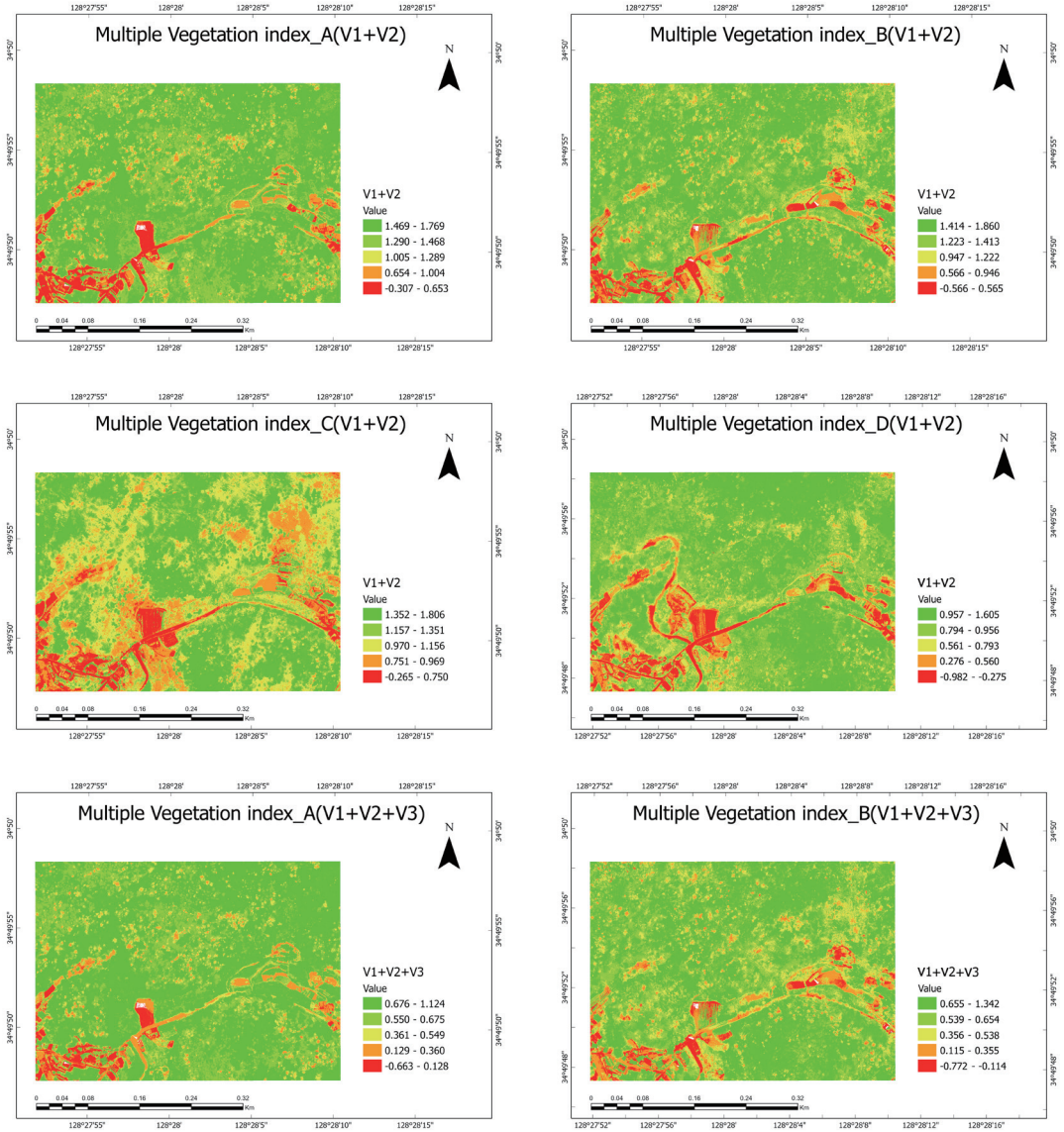

Fig. 6. (Color online) Multivegetation index combinations (Groups 2 and 3).

Table 3
Analysis of multivegetation indices. (unit: m^2)

Period	Vegetation level	Vegetation index										
		(1)	(2)	(3)	(4)	(5)	(6)	(7)	(8)	(9)	(10)	(11)
A	L5	75667	21914	65565	905	72354	12067	88070	80331	41493	45442	73261
	L4	55584	75361	56145	52371	48312	43356	46808	46769	71377	62390	53743
	L3	13446	47102	18223	86105	19209	59477	11616	15027	27504	29136	16281
	L2	8020	12482	19090	19410	12759	34626	9016	11124	14691	16858	11457
	L1	7237	3092	928	1283	7318	10427	4442	6701	4887	6125	5210
B	L5	63717	25047	17117	2086	2175	3644	61575	63158	1479	1361	831
	L4	57015	101617	69524	20813	23098	8199	57141	55941	8513	5804	44186
	L3	22362	6654	52625	78568	80479	19981	24567	23147	33261	17732	78692
	L2	10303	21290	16476	50016	45553	62171	11524	12146	70389	72511	29591
	L1	6556	5451	4189	8594	8742	66053	5151	5540	46280	62639	6630
C	L5	42894	42280	27294	1175	22630	827	42335	29390	26437	1463	29301
	L4	39129	37550	33665	21279	32877	18062	39196	35828	34159	30667	35981
	L3	43429	41028	38552	79661	40257	42074	43803	40971	41174	47184	42284
	L2	24145	32274	42070	53902	50804	65787	26463	39596	45992	59830	43264
	L1	10459	6900	18452	4041	13488	33307	8236	14249	12271	20912	9204
D	L5	59361	73165	54145	5576	47133	14400	67793	57585	56062	1238	62065
	L4	60637	51370	51117	17590	53929	46872	59931	52934	52997	64602	53712
	L3	19634	21260	27559	46784	32086	52640	18735	25271	30456	61872	25869
	L2	11006	13480	14154	66525	18089	39076	12677	13424	19594	31258	17316
	L1	9454	817	13117	23617	8855	7104	957	10879	982	1123	1071

A is characterized by summer, which is the growth season, and is commonly characterized by the overall increase in vegetation vitality. In Period B, combinations (4), (6), (9), and (10) showed that the healthy vegetation area was relatively low. This period is characterized by a gradual decrease in photosynthetic activity and a reduction in chlorophyll content, resulting in a general decline in vegetation vitality. In Period C, the healthy vegetation areas of (1), (2), and (7) were relatively high, but vegetation vitality was generally low. In Period D, the healthy vegetation area was high, at approximately 73%, in combinations (1), (2), (7), and (11). This indicates that the vitality area in Period D significantly increased compared with that in Period C, suggesting that vegetation showed rapid growth.

Figure 7 shows the multivegetation index area combinations in a manner that facilitates the intuitive identification of combinations exhibiting high (green) and low values. This enables the comparison of trends and differences between the combinations or healthy vegetation area (L4 + L5) in Periods A, B, C, and D. The analysis shows high vegetation vitality for (1), (2), (3), (7), (8), and (11) in Periods A, B, and D.

3.3 Analysis of *CVI*

The analysis of *CVI* was based on the results of the basic vegetation indices and multivegetation index combinations. A total of 44 combinations were analyzed, and Table 4 presents the results, which are arranged in descending order of the percentage of healthy

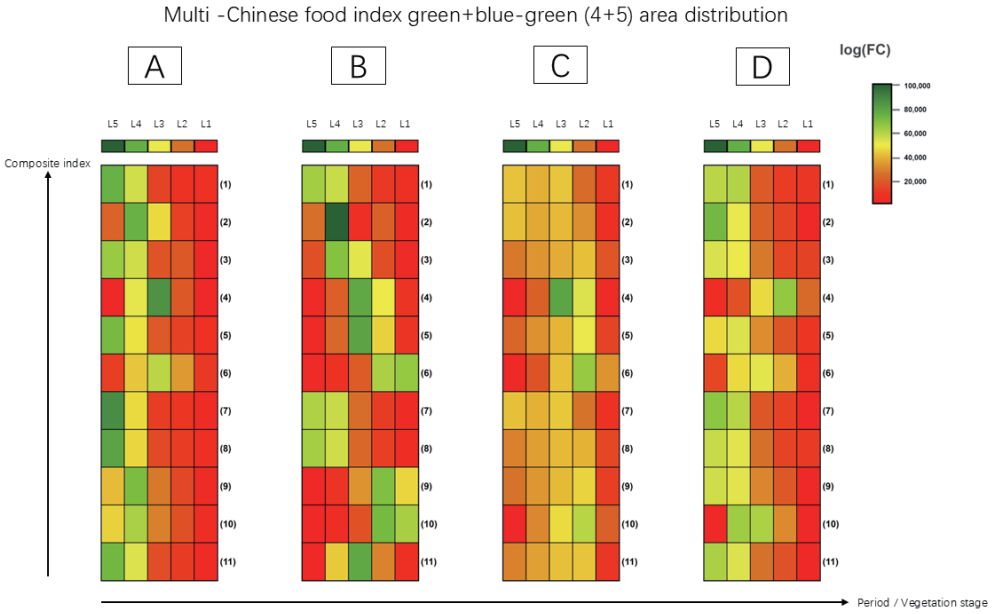

Fig. 7. (Color online) Multivegetation indices (Groups 2 and 3).

Table 4
Analysis results of *CVI*.

Rank	Period	Combination formula	Area (m^2)	Ratio (%)
1	A	(7)	134878	84
2	A	(1)	131251	82
3	D	(7)	127724	80
4	A	(8)	127100	79
5	A	(11)	127004	79
6	B	(2)	126664	79
7	D	(2)	124535	78
8	A	(3)	121710	76
9	B	(1)	120732	75
10	A	(5)	120666	75
⋮	⋮	⋮	⋮	⋮
35	B	(11)	45017	28
36	C	(10)	32130	20
37	B	(5)	25273	16
38	D	(4)	23166	14
39	B	(4)	22899	14
40	C	(4)	22454	14
41	C	(6)	18889	12
42	B	(6)	11843	7
43	B	(9)	9992	6
44	B	(10)	7165	4

vegetation area. As presented in Table 4, three combinations had a healthy vegetation area exceeding 80%, and 10 combinations had a healthy index above 75%. Considering the *CVI* characteristics of the study area, we found relatively high connectivity among Periods A, B, and

D and combinations (1), (2), and (7). Additionally, the vegetation indices $V1$ and $V2$ that correspond to combinations (1) and (7) were high, indicating that they best represent vegetation vitality. Seasonal factors indicate that vegetation vitality is highest from late spring to summer (May to August); thus, applying the vegetation combination equation [Eq. (7)] during this period will provide relatively more reliable vegetation indices.

The optimal *CVI* for the study area was determined to be (7), and our analysis indicates that combining the vegetation indices $V1$, $V2$, and $V3$ ($V1 + V2 + V3$) is effective. By combining indices that measure different physiological aspects (vitality, chlorophyll, and water content), the combination equation [Eq. (7)] facilitates the appropriate representation of comprehensive, multifaceted vegetation status information, which is difficult to obtain with a single index or a combination of two indices. The optimal *CVI* equation in this study is expressed in Eq. (5).

$$CVI(7) = NDVI + RENDVI + NDWI = \frac{NIR - RED}{NIR + RED} + \frac{NIR - Red\ Edge}{NIR + Red\ Edge} + \frac{Green - NIR}{Green + NIR} \quad (5)$$

4. Discussion

CVI(7) achieves a correction effect by applying the water constraint factor, using $V3$, to the data on photosynthetic potential and efficiency provided by $V1$ and $V2$. This means that even if the physiological signals from $V1$ and $V2$ are elevated, the index more accurately captures the decrease in plant vitality caused by severe environmental stress, such as water scarcity, which is indicated by low $V3$ values. As a result, *CVI*(7) can evaluate the health of the *Pinus thunbergii* forest in the study area more thoroughly and accurately than individual indices alone.[22–25]

5. Conclusions

In this research, we focused on evaluating the healthy vegetation zones (L4 + L5) over different periods, vegetation indexes, and vegetation levels. We utilized multisensor data gathered from drones specific to the experimental location in Hwado. Afterward, we proposed the ideal *CVI*.

The analysis of the 16 basic vegetation indices utilized in the experiment, combined with the 44 vegetation vitality distributions calculated from the 11 combination equations for Groups 2 and 3, resulted in the following conclusions.

During Period A, $V1$ (92234 m^2) and $V2$ (84300 m^2) both exhibited significant levels of vitality. Throughout Periods C and D, Index $V2$ showed a marginally higher vitality than $V1$. The conclusion reached can be attributed to the intense photosynthetic activity observed in plants during Periods A and B, as well as the indices' ability to accurately represent the characteristics of the sensor data. Conversely, low vegetation vitality was observed for $V3$ during Period A, for both $V3$ and $V4$ during Period B, and once again for $V3$ in both Periods C and D.

The qualitative and quantitative analyses of the 44 combination equations revealed significant seasonal variations in vegetation health. The combinations (1), (7), and (11), which included $V1$ during Period A, were identified as having a healthy vegetation area (L4 + L5) totaling 80% or

more in each case. In contrast, Period B showed generally low vitality because of a decline in photosynthetic activity and a decrease in chlorophyll content.

By calculating different vegetation indices and examining regions with healthy plant growth, we were able to determine the optimal *CVI* for the experimental site. The usual indicators in the high-vitality *CVI* are *V*1 and *V*2. Given that the combination in Eq. (7) resulted in the highest value, we have determined that *CVI* = (7) is the optimal vegetation index.

The *CVI* analysis method proposed in this study can overcome the limitations of traditional single vegetation indices, allowing for the more accurate and effective monitoring of changes in vegetation health and area. This method, which makes use of multiple sensors, will assist in the early and effective monitoring of seasonal forest vegetation growth and the detection of forest diseases, including PWD.

However, a limitation of this study is that the determination of the optimal *CVI*(7) was based solely on the internal metric of the "healthy vegetation area ratio". The optimal *CVI*(7) was not thoroughly validated using actual ground truth data or independent statistical performance metrics such as RMSE and R-squared. Therefore, at this stage, *CVI*(7) is considered more of a site-specific vegetation vitality indicator specialized for the Hwado region, rather than a method suitable for universal application.

Future research should focus on integrating various fields of study and multidimensional vegetation indices by utilizing artificial intelligence learning techniques. To ensure the statistical reliability and generalizability of *CVI*(7), it is essential to perform cross-validation using field-measured physiological variables of vegetation. Moreover, further research is needed to extend the application of the index to larger areas, facilitating the development of quicker and more accurate large-scale vegetation health maps.

Acknowledgments

This research was supported by the Green Restoration Specialized Graduate Program through the Korea Environmental Industry & Technology Institute (KEITI) funded by the Ministry of Environment (MOE).

References

1 J. Franklin, J. Serra-Diaz, A. Syphard, and H. Regan: Proc. Natl. Acad. Sci. **113** (2016) 3725. https://doi.org/10.1073/pnas.1519911113
2 K. Mehmood, S. A. Anees, S. Muhammad, K. Hussain, F. Shahzad, Q. Liu, M. J. Ansari, S. A. Alharbi, and W. R. Khan: Sci. Rep. **14** (2024) 11775. https://doi.org/10.1038/s41598-024-62464-7
3 U. Gulma and A. Abubakar: Int. J. Sci. Res. Arch. **13** (2024) 2277. https://doi.org/10.30574/ijsra.2024.13.2.2277
4 B. Sparrow, J. Foulkes, G. Wardle, E. Leitch, S. Caddy-Retalic, S. Van Leeuwen, A. Tokmakoff, N. Thurgate, G. Guerin, and A. Lowe: Front. Ecol. Evol. (2020). https://doi.org/10.3389/fevo.2020.00157
5 Z. Zhang, C. Hu, Z. Wu, Z. Zhang, S. Yang, and W. Yang: Sci. Rep. **13** (2023) 8031. https://doi.org/10.1038/s41598-023-35152-1
6 S. Lee, S. J. Park, G. M. Baek, H. B. Kim, and C. W. Lee: Korean J. Remote Sens. **35** (2019) 359. https://doi.org/10.7780/kjrs.2019.35.3.2
7 M. Gomez Selvaraj, A. Vergara, F. Montenegro, H. A. Ruiz, N. Safari, D. Raymaekers, and G. Blomme: ISPRS J. Photogramm. Remote Sens. **169** (2020) 110. https://doi.org/10.1016/j.isprsjprs.2020.08.025
8 M. J. Kim, H. S. Bang, and J. W. Lee: J. Korean Forest Soc. **106** (2017) 100. https://doi.org/10.14578/JKFS.2017.106.1.100

9 R. Yu, Y. Luo, Q. Zhou, X. Zhang, D. Wu, and L. Ren: Int. J. Appl. Earth Obs. Geoinf. 101 (2021) 102363. https://doi.org/10.1016/j.jag.2021.102363
10 S. H. Kim, K. W. Kwon, and J. H. Kim: J. Korean Soc. Surv. Geod. Photogramm. Cartogr. **40** (2022) 251. https://doi.org/10.7848/ksgpc.2022.40.4.251
11 J. M. Jung, S. Yoon, J. Hwang, Y. Park, and W. H. Lee: Forest Ecol. Manag. **553** (2024) 121612. http://dx.doi.org/10.1016/j.foreco.2023.121612
12 R. Yu, Y. Luo, and L. Ren: Forest Ecol. Manag. **497** (2021) 119493. http://dx.doi.org/10.1016/j.foreco.2021.119493
13 R. Yu, Y. Luo, and L. Ren: Ecol. Indic. **162** (2024) 112034. https://doi.org/10.1016/j.ecolind.2024.112034
14 K. Zhang, J. Deng, C. Zhou, J. Liu, X. Lv, Y. Wang, and J. Shang: Int. J. Appl. Earth Obs. Geoinf. **135** (2024) 104262. https://doi.org/10.1016/j.jag.2024.104262
15 S. H. Kim, K. W. Kwon, and J. H. Kim: J. Korean Soc. Surv. Geod. Photogramm. Cartogr. **40** (2022) 251. https://doi.org/10.7848/ksgpc.2022.40.4.251
16 J. M. Jung, S. Yoon, J. Hwang, Y. Park, and W. H. Lee: Forest Ecol. Manag. **553** (2024) 121612. http://dx.doi.org/10.1016/j.foreco.2023.121612
17 Z. R. Zhang, J. You, B. J. Kim, J. Sun, and J. W. Lee: Smart Media J. **9** (2020) 46. https://doi.org/10.30693/SMJ.2020.9.3.46
18 B. C. Gao: Remote Sens. Environ. **58** (1996) 257. https://doi.org/10.1016/S0034-4257(96)00067-3
19 J. A. Gamon, J. Peñuelas, and C. B. Field: Remote Sens. Environ. **41** (1992) 35. https://doi.org/10.1016/0034-4257(92)90059-S
20 A. Viña, A. Gitelson, A. Nguy-Robertson, and Y. Peng: Remote Sens. Environ. **115** (2011) 3468. https://doi.org/10.1016/j.rse.2011.08.010
21 C. Zhang, I. Filella, M. Garbulsky, and J. Peñuelas: Remote Sens. **8** (2016) 677. https://doi.org/10.3390/rs8090677
22 T. S. Le, B. Dell, and R. Harper: Forests **15** (2024) 915. https://doi.org/10.3390/f15060915
23 D. Marusig, F. Petruzzellis, M. Tomasella, R. Napolitano, A. Altobelli, and A. Nardini: Forests **11** (2020) 77. https://doi.org/10.3390/f11010077
24 J. Zurita, R. Garrido, M. Solano, and X. Núñez: Sapienza: Int. J. Interdiscipl. Stud. **5** (2024) 732. https://doi.org/10.51798/sijis.v5i1.732
25 A. Młynarczyk, M. Konatowska, S. Królewicz, P. Rutkowski, J. Piekarczyk, and W. Kowalewski: Remote Sens. **14** (2022) 4267. https://doi.org/10.3390/rs14174267

About the Authors

Yong-Suk Kim obtained his Ph.D. degree in engineering from Dong-A University, South Korea. He is currently a professor in the Department of Landscape Architecture at the College of Design and Environmental Studies of Dong-A University. His research interests include GIS, GPS, drone convergence technology, hyperspectral and multispectral analyses, vegetation information, and drone-based water quality monitoring. (rosekys@dau.ac.kr)

DoYoung Jung received his M.S. degree in Transportation Engineering from the University of Seoul, Seoul, South Korea, and his Ph.D. degree in Transportation Engineering from Ajou University, Suwon-si, Gyeonggi-do, South Korea, in 2022. Since 2014, he has been a principal researcher at the Korea Institute of Civil Engineering and Building Technology (KICT), Goyang-si, Gyeonggi-do, South Korea. His research interests include transportation engineering, intelligent transportation systems (ITS), autonomous driving, and traffic safety. (jdy@kict.re.kr)

LongYi Zhang joined the master's and doctoral program at Dong-A University in 2024. His research interests include ecological restoration, remote sensing, drones, and GIS. (2477591@donga.ac.kr)